LIMNOLOGY
and
OCEANOGRAPHY

ASLO

Limnol. Oceanogr. 9999, 2020, 1–16

doi: 10.1002/lno.11677

Solar radiation and solar radiation driven cycles in warming and freshwater discharge control seasonal and inter-annual phytoplankton chlorophyll *a* and taxonomic composition in a high Arctic fjord (Kongsfjorden, Spitsbergen)

Willem H. van de Poll,[1*] **Douwe S. Maat**,[2] **Philipp Fischer**,[3] **Ronald J. W. Visser**,[1] **Corina P. D. Brussaard**,[2] **Anita G. J. Buma**[1]

[1]Department of Ocean Ecosystems, Energy and Sustainability Research Institute Groningen, University of Groningen, Groningen, The Netherlands
[2]Department of Marine Microbiology and Biogeochemistry, NIOZ Royal Netherlands Institute for Sea Research and Utrecht University, Texel, The Netherlands
[3]Biosciences, Shelf Sea System Ecology, Alfred Wegener Institute, Germany

Abstract

Fjords on the west coast of Spitsbergen experience variable Arctic and Atlantic climate signals that drive seasonal and inter-annual variability of phytoplankton productivity and composition, by mechanisms that are not fully resolved. To this end, a time series (2013–2018) of Kongsfjorden (N 78°54.2, E 11°54.0) phytoplankton pigments, ocean physics, nutrient concentrations, and microbial abundances was investigated. Kongsfjorden phytoplankton dynamics were predominantly governed by solar radiation and cycles of warming and freshwater discharge that caused pronounced changes in light and nutrient availability. Phytoplankton growth after the polar night commenced in March in a mixed, nutrient loaded water column, and accelerated in April after weak thermal stratification. Spring (weeks 10–22) showed high diatom relative abundance that ceased when silicic acid and nitrate reached limiting concentrations. Summer (weeks 23–35) was characterized by sixfold stronger stratification due to increased freshwater discharge and continued ocean heating. This caused a warm, low salinity surface layer with low nutrient concentrations. Small and diverse flagellates, together with high bacterial and viral abundances, thrived in this regenerative, N or P-limited system. Elevated late summer chlorophyll *a* (Chl *a*), and ammonium suggested increased regeneration and nutrient pulses by glacial upwelling. Fall (weeks 36–48) caused rapidly declining Chl *a* and increasing diatom relative abundance, which persisted throughout the polar night, causing high diatom relative abundance during spring. Despite inter-annual variability in ocean temperature and salinity we observed relatively stable seasonal phytoplankton taxonomic composition and Chl *a*.

The seasonality of phytoplankton productivity in the high latitude North Atlantic has captured the interest of researchers for decades. On the west coast of Spitsbergen Atlantic and Arctic conditions interact, resulting in variable water masses of which the consequences for phytoplankton blooms are not fully understood (Kortsch et al. 2012; Soltwedel et al. 2016; Sundby et al. 2016). Furthermore, the high latitude of this location causes strong fluctuations in solar elevation, alternating between 3 months of near darkness during the polar night, and 3 months of midnight sun during summer. As a consequence, fjords such as Kongsfjorden, experience strong seasonality and inter-annual variability in physical–chemical conditions, in, i.e., nutrient concentrations, sea ice cover, freshwater discharge by marine terminating glaciers, ocean temperature, and water column stratification (Tverberg et al. 2019). The warm Atlantic current (west Spitsbergen current, WSC) is an important local heat source causing relatively mild conditions on the west coast of Spitsbergen. On the continental shelf the warm and saline WSC interacts with a fresher and colder coastal current (Spitsbergen polar current, SPC), and with locally altered water. The heat content and salinity of the Atlantic water of the WSC showed positive trends during 1996–2014 (Tverberg et al. 2019), in agreement with the general warming trend of the high latitude North

*Correspondence: w.h.van.de.poll@rug.nl

Additional Supporting Information may be found in the online version of this article.

Atlantic (Soltwedel et al. 2016; Sundby et al. 2016). The colder and fresher SPC has varying characteristics, which most likely depend on upstream sea ice cover (Tverberg et al. 2019). WSC and SPC density, glacial upwelling, and wind forcing influence the inflow of Atlantic water in the fjord, which can occur year round but is most pronounced in summer (Sundfjord et al. 2017). As a consequence the inflow of prevailing water masses varies and consequently the temperature, salinity, and sea ice cover in the fjord show pronounced inter-annual variability. Furthermore, significant positive trends of mean annual and seasonal air temperature have been observed due to climate change on Spitsbergen, with the strongest temperature increases in winter (Maturilli et al. 2019). Combined, these changes have increased Kongsfjorden heat content, resulting in reduced late-winter and early-spring land fast ice thickness and cover, and increased summertime glacial melting and terrestrial freshwater discharge (Guruvayoorappan et al. 2020; Hop et al. 2019; Pavlova et al. 2019). Currently it is largely unclear how these changes influence phytoplankton productivity and composition in Kongsfjorden. It has been suggested that changes in sea ice and hydrographic conditions during 2003–2016 may have altered the biogeochemical controls of phytoplankton blooms. Reduced sea ice may have changed the production regime of ice algae and early diatom blooms towards later blooms of flagellates (Hegseth and Tverberg 2013; Hegseth et al. 2019). Furthermore, summertime stratification in the fjord may have increased as a result of increased glacial discharge causing reduced light availability and nutrient limitation (Piquet et al. 2014; Poll et al. 2018). However, many of these conceptual schemes are based on a limited number of observations, or observations biased towards relatively short periods in the summer months. Therefore, the magnitude of these effects remains unclear. Accurate assessment of these changes requires a thorough understanding of the drivers of phytoplankton biomass and composition in this system. We produced a time series (2013–2018) of year round oceanographic variables (ocean temperature, salinity) at the AWIPEV underwater observatory on the southern shore of central Kongsfjorden. In addition, phytoplankton pigments, nutrient concentrations, and microbial abundances (i.e., flow cytometric detection of small phytoplankton, bacteria and viruses) were sampled on a weekly basis. The goal was to increase our understanding of the major drivers of seasonal and inter-annual variability in phytoplankton development and composition.

Methods

The ferry box system of the AWIPEV underwater observatory on the southern shore of Kongsfjorden obtains water from ~ 12 m depth in front of the "Old Pier" of Ny Ålesund (N 78°54.2, E 11°54.0) (Fischer et al. 2016, 2020). This site was free of sea ice cover during the investigated years, which was low and confined to the sheltered northern inner fjord (Pavlova et al. 2019). Oceanographic (ocean temperature, salinity, turbidity) and biological (chlorophyll a fluorescence) variables were measured by the underwater observatory sensors (Seabird SBE 38 temperature sensor, SBE 45 ADM conductivity sensor, Sea point turbidity sensor, Sea point chlorophyll a fluorescence sensor). We used weekly averaged data collected for the years 2013–2018. Data of the AWIPEV underwater observatory were not continuous due to damage of water input tubes by icebergs and subsequent maintenance, causing data gaps during 2017 (weeks 25, 26, and 30, 31) and 2015 (weeks 19–28). In addition, winter and early spring low salinity anomalies were removed, assuming these were caused by stranded icebergs close to the sensors of the observatory (2017 week 11; 2016 weeks 5–7; 2015 weeks 2–4; 2013 week 10). Additional seawater samples (10 liter) for phytoplankton pigments, nutrient concentrations, and microbial abundances were collected from the underwater observatory via a bypass of the ferry box water support. In case of ferry box system malfunctions, discrete water samples were collected in front of the "Old Pier" close to the ferry box pump site by Niskin bottle or bucket. Pigment water samples were collected (semi) weekly from October 2013 to July 2018, resulting in 259 discrete samples, covering 218 weeks. Nutrient samples (nitrate, phosphate, nitrite, ammonium, silicic acid) were collected between April–June, 2014, and June 2015–July 2018, providing 189 samples, covering 148 weeks. Samples for microbial abundances were collected from April 2015 to July 2016, resulting in 103 samples for 103 weeks. All hydrographical data, nutrients, and biological samples were collected at 12 m at the underwater observatory site and were therefore assumed to be characteristic for the surface ocean of the southern shore of central Kongsfjorden (van de Poll et al. 2016, Hop et al. 2019, Hop and Wiencke 2019).

Phytoplankton pigment and CHEMTAX analysis

Seawater (4–10 liter) was filtered on 47 mm GF/F (Whatman) filters for pigment analysis using mild over pressure (0.2 bar, 20 kPa). Filtration was stopped after 30 min, and filtered water volume was recorded. Afterwards filters were snap frozen in liquid nitrogen and stored at – 80°C until High Performance Liquid Chromatography (HPLC) pigment analysis. Filters were freeze dried for 48 h before pigment extraction in 90% acetone (v/v) for 48 h (4°C, darkness) (van Leeuwe et al. 2006). Pigments were separated by HPLC (Waters 2695) with a Zorbax Eclipse XDB-C8 column (3.5 μm particle size), using a method based on Van Heukelem and Thomas (2001). Detection was based on retention time and diode array spectroscopy (Waters 996) at 436 nm. Pigments were manually quantified using standards for all used pigments (DHI lab products). All chlorophyll a concentrations in figures and text were determined by HPLC, with a detection limit of ~ 0.005 mg Chl a m^{-3}. Absolute and relative abundances of phytoplankton groups were assessed by CHEMTAX (version

1.95) (Mackey et al. 1996), which used factor analysis and a steepest descent algorithm to partition pigments between groups, using initial pigment ratios (Table S1). Included groups were prasinophytes, cryptophytes, haptophytes, pelagophytes, silicoflagellates, dinoflagellates, and diatoms. CHEMTAX was performed separately for samples with high (> 0.1 mg m^{-3}) and low (< 0.1 mg m^{-3}) Chl *a*. All pigments were allowed to vary during CHEMTAX analysis (Chl *a*: 100%, fucoxanthin: 10%, other pigments: 500%). Initial and final pigment ratios are presented in Table S1. Haptophytes and pelagophytes showed highly similar dynamics and were pooled as haptophytes. Final pigment ratios were in agreement with reported values of the respective taxonomic groups (Higgins et al. 2011).

Nutrients

Filtered (0.2 μm Acrodisc, Pall) subsamples (5 mL) for dissolved inorganic nutrient analyses were stored at – 20°C (phosphate, ammonium, nitrate and nitrite) or 4°C (silicic acid). Nutrient analyses were conducted using a Traacs 800 autoanalyzer (Bran and Luebbe) according to Murphy and Riley (1962), Helder and De Vries (1979), and Grasshoff (1983). Detection limits were 0.01, 0.03, 0.02, and 0.26 μM for phosphate, ammonium, nitrate and nitrite, and silicic acid, respectively.

Microbial abundances

The abundances of small phytoplankton (< 20 μm), bacteria and viruses were determined using a BD FACSCalibur benchtop flow cytometer (BD Biosciences, San Jose, CA) with 15 mW argon laser. Upon sampling, 3.5 mL of seawater was fixed with formaldehyde (0.5% final concentration; Sigma-Aldrich, St. Louis, MO) for phytoplankton abundances and 1 mL was fixed with glutaraldehyde (0.5% final concentration; EM-grade; Sigma-Aldrich) for enumeration of bacteria and viruses. After 30 min, samples were flash frozen in liquid nitrogen and stored at – 80°C until analysis. Phytoplankton abundances were determined with a red (Chl *a*) fluorescence trigger (Marie et al. 2001). Bacteria and virus samples were diluted in 0.2 μm filtered (FP 30/0.2 CA-S Whatman, Dasser, Germany) TE-buffer (pH 8.2) and stained for 10 min at 80°C with nucleic acid-specific SYBR Green I (Invitrogen Molecular Probes, Eugene, OR, USA) according Brussaard (2004). Afterwards, bacteria and viruses were enumerated with a green fluorescence trigger. Total abundances (per mL) of phytoplankton, bacteria, and viruses were calculated with the program FCS express 5 (De Novo Software, Glendale 275, CA).

Meteorological data

Solar irradiance (370–695 nm, W m^{-2}) in Ny Ålesund was retrieved by subtracting filtered irradiance measurements from the broadband global radiation measurements that contribute to the Baseline Surface Radiation Network (BSRN), similar to Maturilli et al. (2019). Surface air temperature at 2 m was observed on the AWI meteorological tower in Ny Ålesund (Maturilli).

Data analysis

Weekly averages of environmental and biological data were used to produce an average annual cycle for the years 2013–2018. Correlations between biological and environmental data of week averages were explored using a principle component analysis (PCA). PCA was performed for the annual cycle and the seasons specified below. The average weekly annual cycle was used to calculate Spearman rank correlation coefficients between ocean physics (ocean temperature, salinity), climate (irradiance, air temperature), nutrient concentrations (phosphate, ammonium, nitrite, nitrate, and silicic acid), and biology (HPLC derived chlorophyll a, phytoplankton composition by CHEMTAX, relative to Chl *a*), and microbial abundances of phytoplankton, bacteria, and viruses, to investigate links between these. We distinguish four (meteorological) seasons: autumn (weeks 36–48), winter (weeks 49–9), the latter two phases include the polar night; spring (weeks 10–22), and summer (weeks 23–35). Furthermore, we investigated inter-annual anomalies of seasonal averages of individual years. Seasonally averaged ocean and air temperature, salinity, and phytoplankton Chl *a* and taxonomic composition were tested for trends. Seasonally grouped week averages of individual years were tested for significance using a rank based ANOVA procedure, and differences between groups were considered significant at $p < 0.05$. Data coverage of nutrient samples and microbial abundances was lower as compared to environmental and pigment data (as specified above). Therefore, these data were not considered for assessing inter-annual variability.

Results

Average annual cycle of environmental variables

Autumn and winter (weeks 36–9)

Most trends of variables with minimum or maximum values at the end of winter and early spring started during week 35 (autumn) and continued throughout the polar night (weeks 43–8) into the first weeks of spring. During weeks 35–50 air temperature dropped by 0.75°C week^{-1} (R^2: 0.99), whereas weeks 51–14 were characterized by more variability and a less pronounced decline (0.32°C week^{-1}, R^2: 0.48, Fig. 1). Ocean temperature declined linearly during weeks 35–50 by 0.26°C week^{-1} (R^2: 0.97). This decline was less pronounced during weeks 51–11 (– 0.14°C week^{-1}, R^2: 0.92). Salinity and density increased linearly (R^2: 0.93) during weeks 35–53 (0.09 PSU week^{-1}), and increased less pronounced up to week 14 of the next year (0.03 week^{-1}, R^2: 0.87). Density correlated with salinity and inversely with ocean temperature during weeks 35–14 (*r*: 0.998, –0.98). Phosphate, nitrate, and silicic acid concentrations increased during weeks 35–14, and correlated inversely with ocean

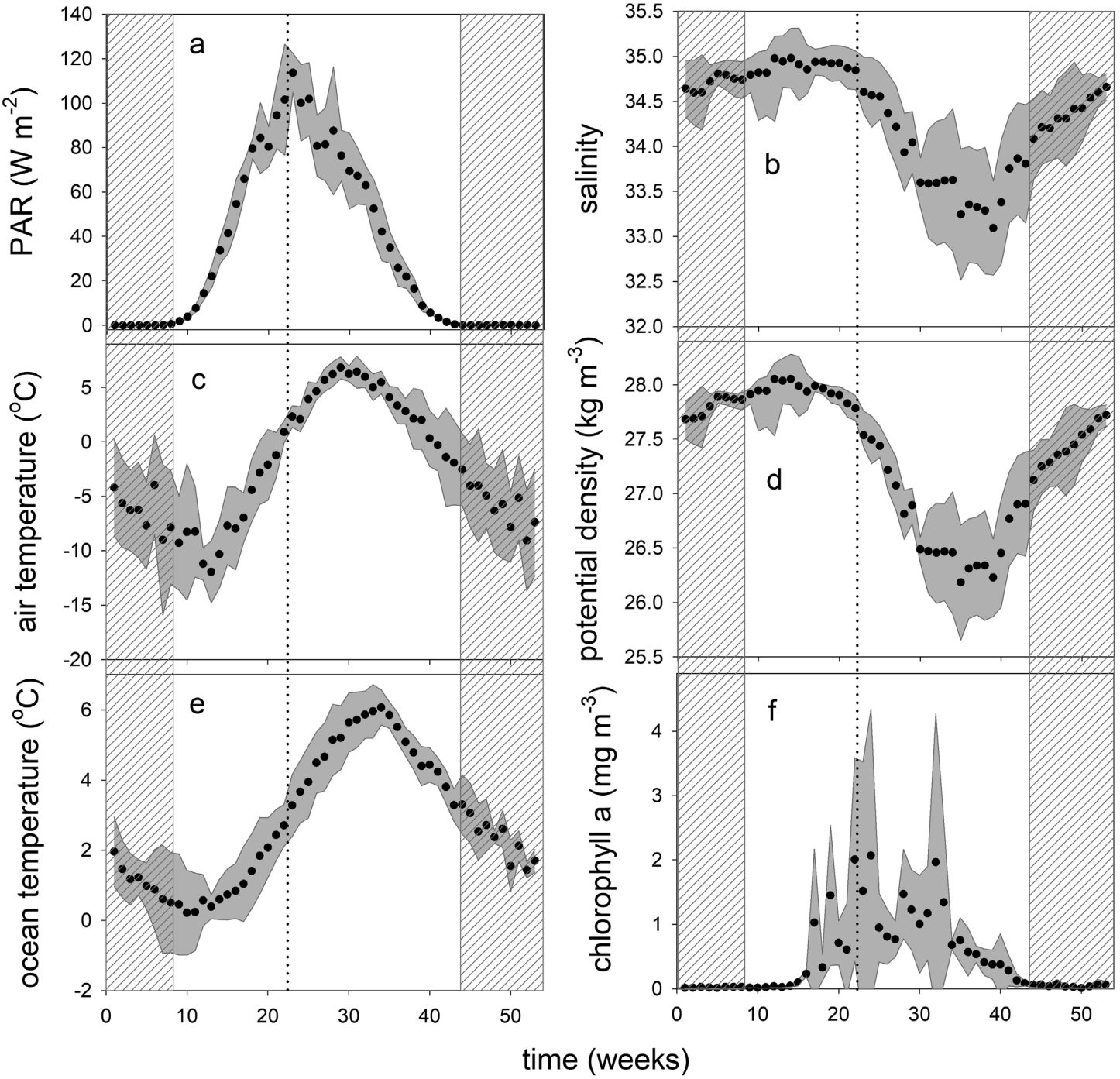

Fig. 1. Irradiance (**a**), salinity (**b**), air temperature (**c**), potential density (**d**), ocean temperature (**e**), and chlorophyll a concentration measured by HPLC (**f**). Data points are week averages over 2013–2018, the gray area represents the standard deviation. The gray pattern indicates the polar night (weeks 43–8). The dotted line separates spring and summer (weeks 22–23). Irradiance and air temperature were measured in Ny Ålesund, ocean temperature, salinity and chlorophyll a samples were collected at the underwater observatory on the southern shore of Kongsfjorden.

temperature (*r*: −0.96, −0.95) and salinity (0.96, 0.95) (Figs. 2 and S1). Nitrite concentrations reached a maximum during the early stages of the polar night (weeks 41–47). Ammonium concentrations showed a declining trend during weeks 35–50. Chlorophyll a concentration declined 17-fold during autumn, and declined at a slower rate during the polar night to minimum concentrations during weeks 1–8 (0.02 ± 0.007 μg Chl *a* m^{-3}, Fig. 1). Phytoplankton, bacterial,

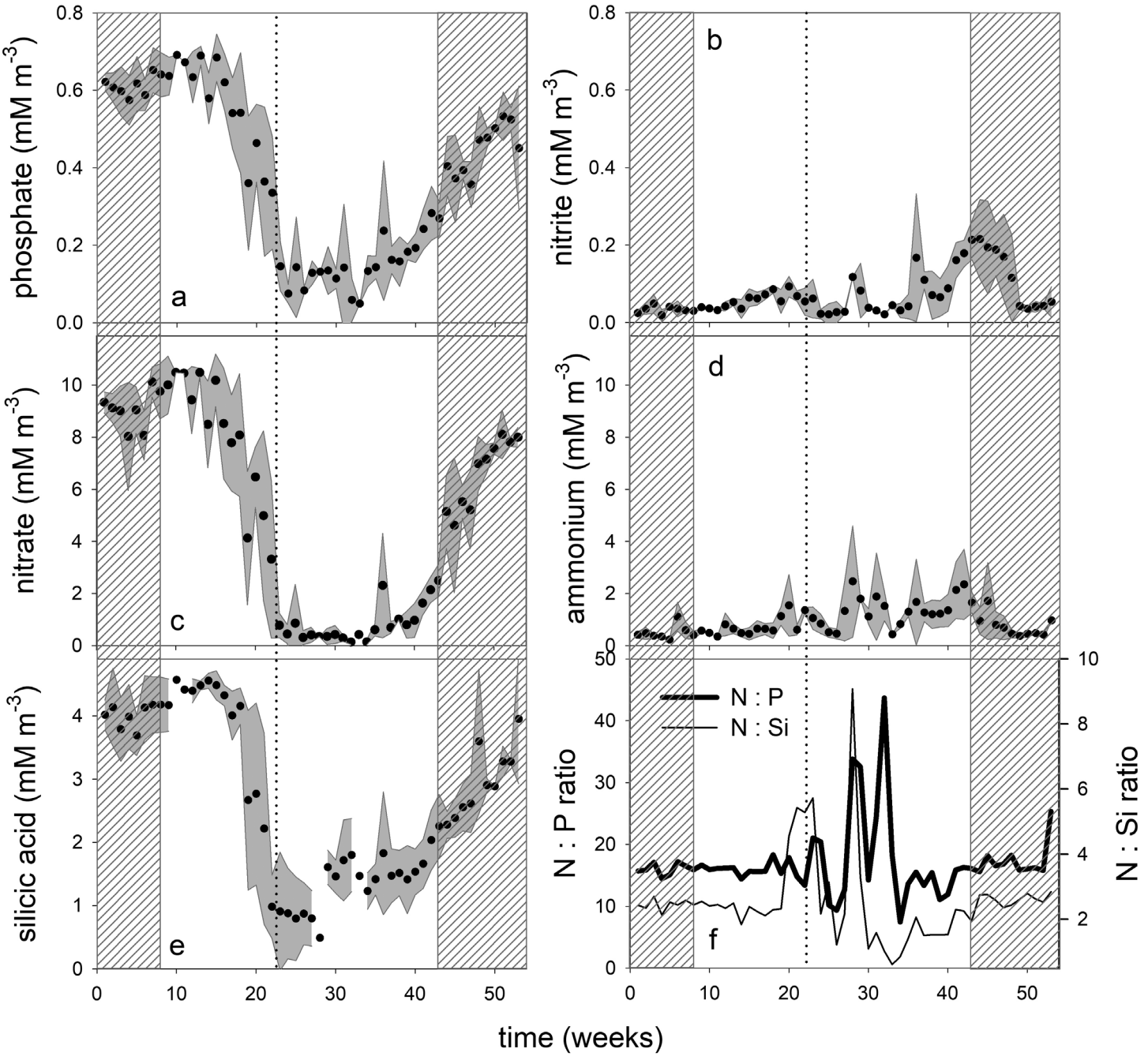

Fig. 2. Concentrations of phosphate (**a**), nitrite (**b**), nitrate (**c**), ammonium (**d**), silicic acid (**e**), and the N : P (nitrate, nitrite, and ammonium relative to phosphate) and N : Si ratio (nitrate, nitrite, and ammonium relative to silicic acid) (**f**) at the underwater observatory on the southern shore of Kongsfjorden. Data points are week averages over 2014–2018, the gray area represents the standard deviation. The gray pattern indicates the polar night (weeks 43–8). The dotted line separates spring and summer (weeks 22–23).

and virus abundances also declined during autumn and the polar night to minimum concentrations during weeks 4–8 (Fig. 3). Phytoplankton abundance declined 17-fold whereas bacterial and virus abundances declined 4- and fivefold, respectively when comparing weeks 35 and 8. Polar night minimum phytoplankton abundances were 200-fold lower as compared to maximal concentrations observed during weeks 31–32, whereas Chl *a* concentration was 100-fold lower than its summer maximum. Bacterial and virus abundances were 12- and fivefold lower, respectively. Turbidity declined from a maximum (week 32) up to week 50 to a minimum during winter and early spring (Fig. S2).

Spring (weeks 10–22)

Increasing irradiance left an increasing imprint on ocean physics and air temperature, and on microbial productivity. Ocean and air temperature reached their annual minimum during weeks 10 and 13, respectively, and increased thereafter (Fig. 1). Salinity and density increased up to week 14, and declined afterwards, suggesting a stratified water column from week 15 onwards. Nutrient concentrations declined after week 14 from their early spring maximum (weeks 10–14: phosphate: 0.65 ± 0.1; nitrate: 9.8 ± 0.1; silicic acid: 4.5 ± 0.2 μmol L^{-1}) (Fig. 2). During weeks 20–23, the average N : Si ratio (nitrate, nitrite, and ammonium relative to silicic acid) increased from 2.3 ± 0.2 (weeks 10–19) to 5.5 ± 0.5, whereas the N : P ratio (nitrate, nitrite, and ammonium relative to phosphate) showed no significant change during spring (15.9 ± 1.0 to 16.8 ± 3.4, Fig. 2). Irradiance correlated positively with ocean and air temperature during weeks 10–22 (r: 0.99, 0.90) (Fig. S3). There was an inverse correlation between ocean temperature and potential density (r: –0.92), whereas salinity showed a positive correlation with density (r: 0.72) during weeks 14–22. Irradiance and ocean temperature relationships increased stronger during weeks 15–22 than during weeks 10–14. During the latter, air temperature was still very low (on average – 9.1°C, Fig. 1). On average, Chl *a* concentration increased exponentially during weeks 10–22 with an accumulation rate of 0.42 $week^{-1}$ (R^2: 0.88), reaching average peak concentrations of 2.0 mg m^{-3}. The accumulation rate was 0.36 $week^{-1}$ using weekly averaged Chl *a* fluorescence of the underwater observatory sensor (R^2: 0.88, not shown). Microbial abundances increased during weeks 15–21 (Fig. 3). Turbidity increased sharply after week 15 (Fig. S2).

Summer (weeks 23–35)

Weekly averaged irradiance (2013–2018) peaked during week 23 and declined afterwards (Fig. 1). Air temperature increased up to week 29, whereas ocean temperature increased up to week 34. As a consequence, salinity declined steeply during week 22 (– 0.11 PSU $week^{-1}$; R^2: 0.92), and reached a minimum during week 35. The inverse correlation between ocean temperature and salinity (r: –0.94) during weeks 23–35 suggested that increasing ocean heat content promoted freshwater discharge (glacial melting) (Fig. S3). Density showed strong correlations with salinity (weeks 23–35: 0.99) and with ocean temperature (– 0.96). During weeks 23–35 concentrations of phosphate (0.11 ± 0.04) and nitrate (0.37 ± 0.20 μmol L^{-1}) were at a minimum. Silicic acid was at a minimum during weeks 22–28 (0.82 ± 0.16 μmol L^{-1}), and increased to 1.7 ± 0.17 μmol L^{-1} afterwards. Summertime ammonium concentrations (1.23 ± 0.7 μmol L^{-1}) were fourfold higher than nitrate concentrations. The average N : P ratio (nitrate, nitrite, and ammonium relative to phosphate) during weeks 23–35 was variable, with 11 weeks above and 22 weeks below the winter and early spring average (16.7 ± 2.6) of our time series (Fig. 2). N : Si (nitrate, nitrite, and ammonium relative to silicic acid) was also variable but on average similar as during winter (2.3 ± 2.3 vs 2.3 ± 0.4, respectively). Summer Chl *a* was variable and showed peaks during early (week 24) and late (week 35) summer, but showed no linear trends (on average 1.2 ± 0.5 μg Chl *a* L^{-1}). Phytoplankton abundance increased

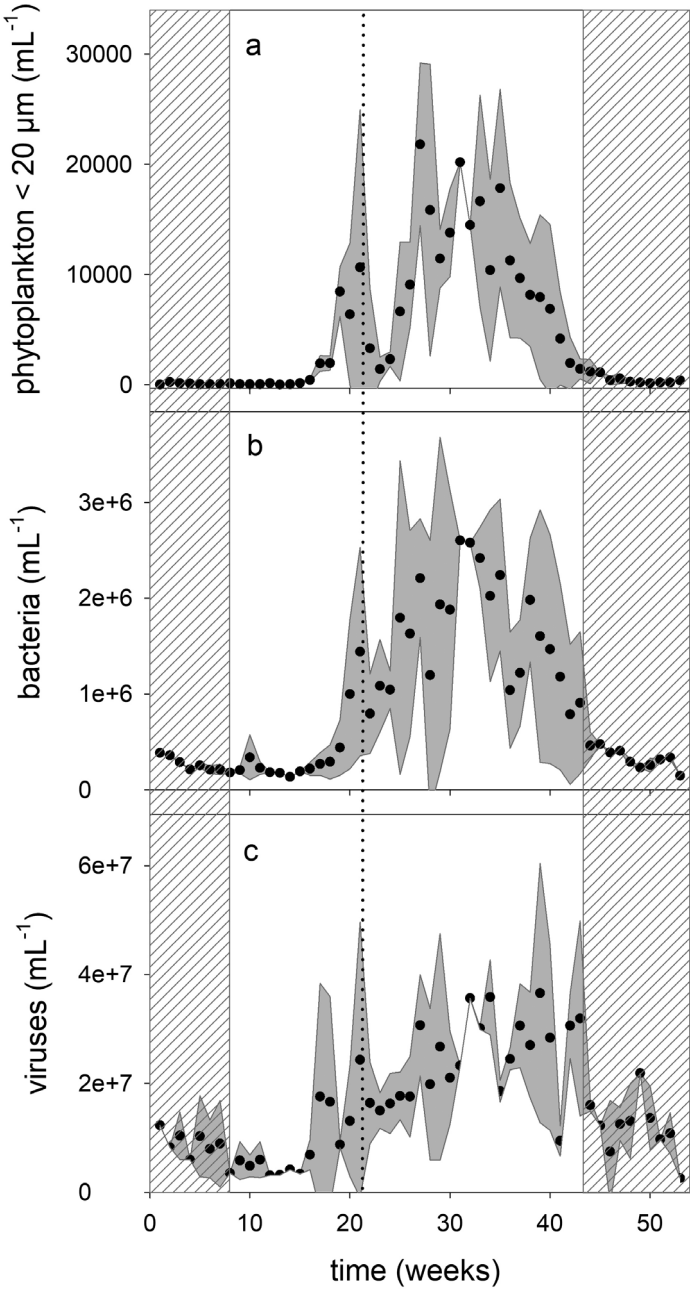

Fig. 3. Abundances determined by flow cytometry of phytoplankton (< 20 μm) (**a**), bacteria (**b**), and viruses (**c**) at the underwater observatory on the southern shore of Kongsfjorden. Data points are week averages over 2014–2015, the gray area represents the standard deviation. The gray pattern indicates the polar night (weeks 43–8). The dotted line separates spring and summer (weeks 22–23).

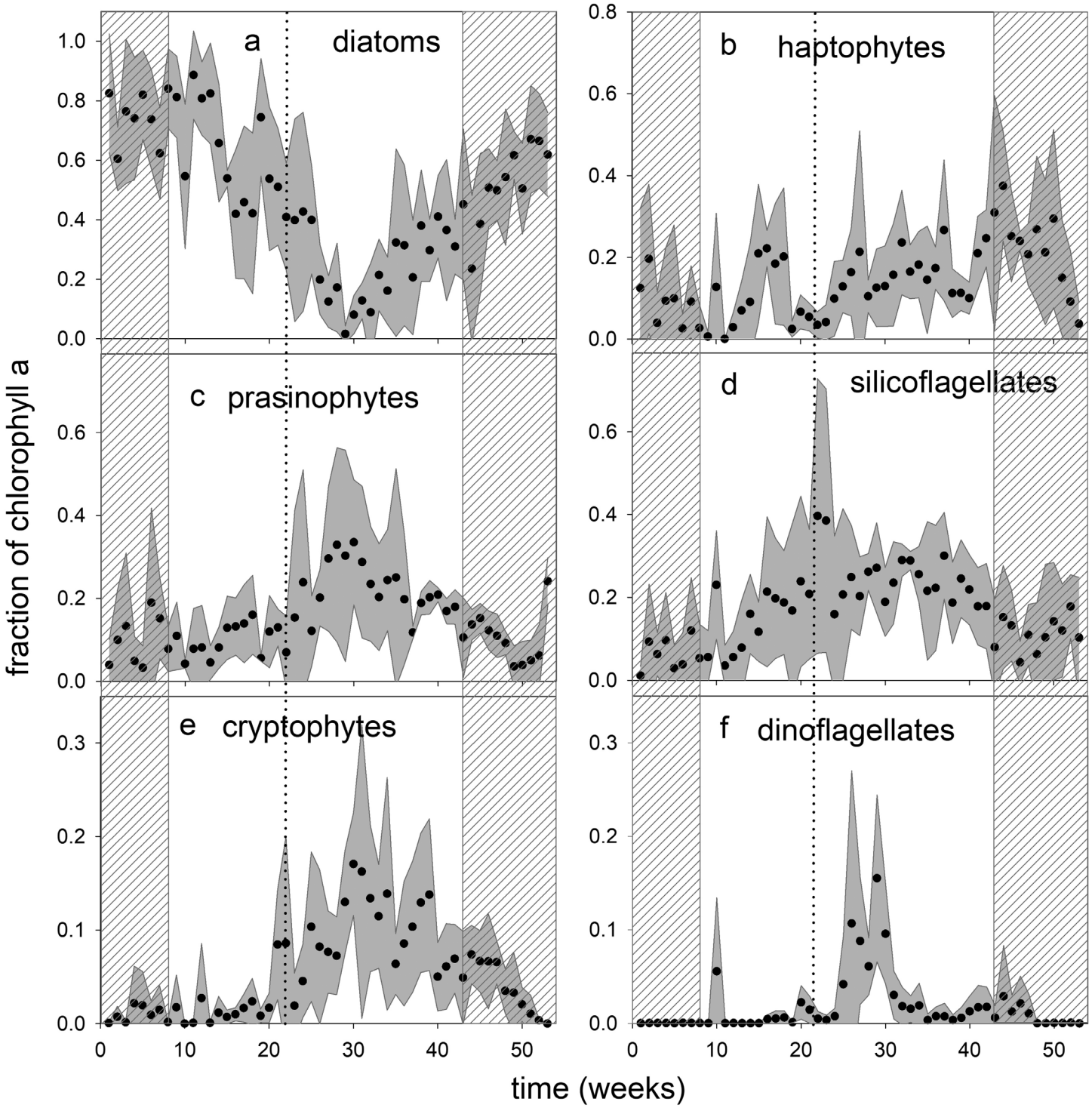

Fig. 4. Relative abundances of diatoms (**a**), haptophytes (**b**), prasinophytes (**c**), silicoflagellates (**d**), cryptophytes (**e**), and dinoflagellates (**f**) at the underwater observatory on the southern shore of Kongsfjorden. Relative abundance is expressed as a fraction of chlorophyll a (0–1). Data points are week averages over 2013–2018, the gray area represents the standard deviation. The gray pattern indicates the polar night (weeks 43–8). The dotted line separates spring and summer (weeks 22–23).

strongly during weeks 24–35, and declined afterwards (Fig. 3). Bacterial and virus abundance peaked during weeks 27–35. Turbidity fluctuated between high and low values during summer (Fig. S2).

Average annual cycle of phytoplankton taxonomic composition

Diatoms showed distinct patterns from other taxonomic groups, with a high share of Chl *a* during the first 9 weeks of the year (average 75 ± 8%), and maintained dominance (60 ± 17% of Chl *a*) during spring (weeks 10–22) (Fig. 4). Diatom relative abundance declined during spring and reached a minimum in summer during week 29 (1.6% of Chl *a*). This was followed by a progressive increase throughout autumn and winter up to week 8 of the next year. Diatom relative abundance correlated positively with nitrate, phosphate, and silicic acid over the average annual cycle, and showed strong inverse correlations with ocean and air temperature (Table 1; Fig. 5). Their relative abundance increased during autumn and winter at the expense of flagellated phytoplankton groups. Flagellated phytoplankton (prasinophytes, cryptophytes,

Table 1. Spearman rank correlations between week averages over 2013–2018 of pigment based taxonomic phytoplankton composition (expressed relative to Chl *a*) and environmental (irradiance, weeks in darkness during polar night), oceanographic (ocean temperature, salinity, potential density) variables, and nutrient concentrations (phosphate, nitrate, silicic acid). Correlations that were not significant are denoted as: ns.

	Diatom	Prasino	Crypto	Hapto	Silico	Dino
Irradiance	−0.52	0.42	0.44	Ns	0.71	0.52
Darkness	0.85	Ns	−0.72	−0.86	Ns	−0.48
Temperature	−0.87	0.69	0.85	0.42	0.66	0.66
Salinity	0.71	−0.56	−0.70	−0.49	−0.38	−0.47
Density	0.76	−0.60	−0.76	−0.46	−0.48	−0.53
Phosphate	0.85	−0.71	−0.82	−0.30	−0.68	−0.69
Nitrate	0.88	−0.70	−0.84	−0.32	−0.72	−0.71
Silicic acid	0.78	−0.60	−0.79	Ns	−0.65	−0.66

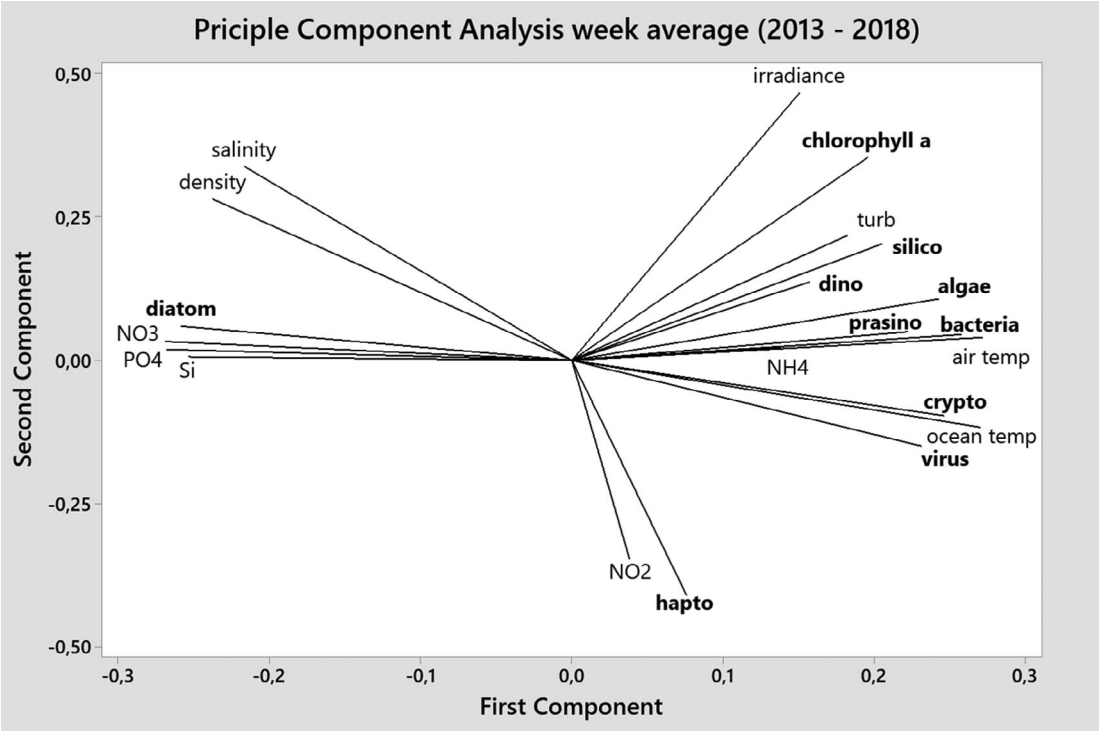

Fig. 5. Principle component analysis of biological (bold) and environmental data of week averages over the average annual cycle (2013–2018). Biological data were HPLC derived chlorophyll a, pigment derived abundance (relative to Chl *a*) of diatoms (diatom), haptophytes (hapto), dinoflagellates (dino), prasinophytes (prasino), cryptophytes (crypto), and silicoflagellates (silico), and flow cytometry derived abundances of algae (< 20 μm), bacteria and viruses. Environmental data were inorganic nutrient concentrations (nitrate: NO_3; phosphate: PO_4, silicic acid: Si; nitrite: NO_2; and ammonium: NH_4), irradiance, salinity, density, ocean temperature (ocean temp), air temperature (air temp), and turbidity (turb).

Table 2. Spearman rank correlations between week averages (2013–2018) of biological variables (Chl *a* of discrete samples, chlorophyll a in situ fluorescence (Chl *a* F), phytoplankton, bacteria, and virus abundances of discrete samples (cells mL^{-1}) and environmental (irradiance, weeks in darkness during polar night), oceanographic (ocean temperature, salinity, potential density) variables, and nutrient concentrations (phosphate, nitrate, silicic acid). Correlations that were not significant are denoted as: Ns.

	Chl *a*	Chl *a* F	Phyto ≤ 20 μm	Bacteria	Viruses
Irradiance	0.82	0.70	0.63	0.51	0.40
Darkness	−0.66	Ns	−0.86	−0.78	−0.66
Temperature	0.71	0.60	0.88	0.91	0.83
Salinity	−0.33	Ns	−0.63	−0.73	−0.71
Density	−0.44	−0.35	−0.72	−0.81	−0.77
Phosphate	−0.81	−0.65	−0.89	−0.89	−0.79
Nitrate	−0.81	−0.67	−0.90	−0.89	−0.81
Silicic acid	−0.75	−0.66	−0.83	−0.87	−0.77

Table 3. Seasonal averages of ocean physics (temperature, °C; salinity), air temperature (°C), and phytoplankton biomass (chlorophyll a, mg m^{-3}) during winter (weeks 49–9), spring (weeks 10–22), summer (weeks 23–35), and autumn (weeks 36–48) over 2013–2018. Standard deviation is shown in brackets, * indicates limited data availability. Bold values and letters correspond to significant differences ($p < 0.05$) between the week averages of the seasonally grouped data.

Year	2014 (a)	2015 (b)	2016 (c)	2017 (d)	2018 (e)
Ocean temperature (weeks 49–9)	1.60 (0.64)	**0.60 (1.14)**	1.12 (0.54)	**2.04 (0.79)**	1.07 (1.57)
Ocean temperature (weeks 10–22)	**1.75 (0.64) e**	−0.12 (0.27)*	1.44 (0.87)	**1.97 (1.11) e**	**0.16 (0.93)**
Ocean temperature (weeks 23–35)	**5.53 (1.12) e**	5.65 (0.82)	5.29 (1.05)	**5.92 (0.63) e**	**4.27 (1.01)**
Ocean temperature (weeks 36–48)	3.66 (1.31)	**2.79 (1.23) c, d**	**4.19 (0.79) b**	**4.25 (1.00) b**	3.28 (1.38)
Ocean salinity (weeks 49–9)	**34.91 (0.08)c, d, e**	34.71 (0.09)*	**34.14 (0.28)a**	**34.51 (0.48)a**	**34.63 (0.12)a**
Ocean salinity (weeks 10–22)	**35.05 (0.04)**	34.39 (0.27)*	**34.84 (0.07)**	35.01 (0.09)	34.91 (0.09)
Ocean salinity (weeks 23–35)	**33.65 (0.36)c**	33.42 (0.67)	**33.91 (0.74)e**	33.90 (0.18)	**33.76 (0.55)**
Ocean salinity (weeks 36–48)	**33.87 (0.27)b, c, d, e**	**33.09 (0.56)a**	**33.46 (0.31)a**	**33.75 (0.55)a**	**33.78 (0.71)a**
Air temperature (weeks 49–9)	−5.22 (4.40)	−8.60 (4.88)	−5.11 (3.63)	−7.94 (4.71)	−5.41 (3.02)
Air temperature (weeks 10–22)	−7.44(4.15)	−4.82 (3.38)	−4.54 (5.01)	−7.77 (5.41)	−5.77 (6.18)
Air temperature (weeks 23–35)	3.91 (1.94)	5.70 (1.93)	5.49 (1.45)	4.79 (1.45)	5.15 (1.55)
Air temperature (weeks 36–48)	**−2.76 (4.47) c**	−0.91 (3.33)	**1.80 (2.18)**	0.32 (4.83)	**−1.74 (3.04) c**
Chlorophyll a (weeks 49–9)	**0.01 (0.01)**	0.02 (0.01)	**0.04 (0.03)**	0.02 (0.01)	0.03 (0.05)
Chlorophyll a (weeks 10–22)	0.64 (1.21)	0.21 (0.12)	0.73 (1.00)	0.37 (0.44)	0.59 (0.81)
Chlorophyll a (weeks 22–35)	1.03 (1.23)	1.02 (0.45)	0.83 (0.44)	1.95 (1.71)	
Chlorophyll a (weeks 36–48)	0.15 (0.22)	**0.40 (0.37)**	**0.10 (0.11)**	0.23 (0.23)	

silicoflagellates, haptophytes, and dinoflagellates) showed increasing relative abundances during spring (weeks 10–22) and dominated the phytoplankton taxonomic composition during summer (silicoflagellates: 24%, prasinophytes: 24%, diatoms: 22%, cryptophytes: 11%, haptophytes: 10%, and dinoflagellates: 9%). Silicoflagellate relative abundance peaked during the transition between spring and summer, whereas prasinophytes, cryptophytes, and dinoflagellates peaked during summer. The latter correlated with ocean temperature, and inversely with nutrient concentrations, whereas silicoflagellates correlated with irradiance and inversely with nutrients (Table 1; Figs. 5 and S3). Haptophytes peaked at the end of the summer and during autumn, and also showed a significant presence at the end of spring. Haptophytes, cryptophytes, and dinoflagellates showed inverse correlations with time spent in the polar night (weeks in darkness, Table 1).

Average annual cycle of Chl *a* and microbial abundance

Over the average annual cycle, Chl *a* (HPLC derived and fluorescence) correlated most strongly with irradiance (*r*: 0.82) and nutrients (inverse; $-0.75 > r > -0.81$), but also with ocean temperature (*r*: 0.71; Table 2, Fig. 5). Phytoplankton abundances showed stronger correlations with ocean temperature (*r*: 0.88), potential density (inverse; *r*: −0.72), and nutrient concentrations (inverse; $-0.83 > r > -0.90$) than Chl *a*, whereas the correlation with irradiance (*r*: 0.63) was lower. Similarly, bacterial abundance correlated strongly with ocean temperature (*r*: 0.91), potential density (inverse, *r*: −0.81), and

nutrient concentration (inverse – 0.87 > r > –0.89; Table 2; Fig. 5). Over the average annual cycle, phytoplankton abundance (< 20 μm) correlated positively with Chl *a* (r: 0.86), cryptophytes (r: 0.80), silicoflagellates (r: 0.77), and prasinophytes (r: 0.73), and inversely with relative abundance of diatoms (r: –0.86). Bacterial abundance correlated with small phytoplankton abundance (r: 0.87), and Chl *a* (r: 0.73, 0.78). Virus abundances showed the strongest correlation with bacterial and phytoplankton abundances (r: 0.83, 0.78, respectively). Turbidity correlated positively with phytoplankton abundance (r: 0.73), and Chl *a* (r: 0.67).

Table 4. Spring bloom onset and termination (week number) of 2014 to 2018 based on nutrient concentrations (spring bloom onset: Decline from early spring maximum concentrations; limitation: nitrate < 0.1 μmol L^{-1}; silicic acid < 1.0 μmol L^{-1}); and chlorophyll a concentration (onset: Chl *a* exceeding 0.1, and 1.0 mg m^{-3} threshold concentrations, respectively).

	NO_3 onset	Limitation	Si onset	Limitation	Chl *a*: >0.1	>1
2014	16	23	16	23	16	21
2015		23		23	24	25
2016	17	25	17	22	16	17
2017	14	24	16	27	15	17
2018	15	23	15	25	15	19

Inter-annual variability 2013–2018

Seasonally averaged spring and summer ocean temperature showed stronger variability between years (1.9°C) than autumn and winter temperature (1.5°C) (Table 3). Significant differences in seasonally grouped week averages of ocean temperature were observed during all seasons. On average 2015 and 2018 showed lower ocean temperatures than 2014, 2016, and 2017. Episodes of week average salinities of > 34.9 (characteristic of Atlantic water, Corttier et al. 2012) were observed in 2013 (weeks 13–20), 2014 (weeks 4–27), 2016 (weeks

Table 5. Seasonally averaged taxonomic composition (expressed as fraction of chlorophyll a) during winter (**A**), spring (**B**), summer (**C**), and autumn (**D**) over 2014–2018. Dinoflagellates are not shown because photosynthetic dinoflagellates were a very small fraction of Chl *a*. Standard deviation is shown in brackets. Bold values and letters correspond to significant differences ($p < 0.05$) between the week averages of the seasonally grouped data.

A: Winter (weeks 49–9)	2014 (a)	2015 (b)	2016 (c)	2017 (d)	2018 (e)
Diatoms	0.53 (0.11)	0.91 (0.11)	0.75 (0.14)	0.63 (0.15)	0.77 (0.12)
Prasinophytes	0.07 (0.10)	0.01 (0.03)	0.15 (0.13)	0.15 (0.12)	0.05 (0.05)
Haptophytes	**0.31 (0.18)[b,c,d]**	**0.03 (0.07)[a]**	**0.04 (0.11)[a]**	**0.06 (0.09)[a]**	0.08 (0.11)
Cryptophytes	0.001 (0.001)	0.002 (0.002)	0.009(0.025)	0.009 (0.014)	0.038 (0.003)
Silicoflagellates	0.09 (0.11)	0.05 (0.07)	0.06 (0.10)	0.16 (0.13)	0.06 (0.06)
B: Spring (weeks 10–22)	**2014**	**2015**	**2016**	**2017**	**2018**
Diatoms	0.55 (0.21)	**0.36 (0.27)**	0.61 (0.24)	**0.82 (0.12)**	0.57 (0.15)
Prasinophytes	0.10 (0.08)	**0.18 (0.09)**	0.08 (0.07)	**0.04 (0.02)**	0.11 (0.06)
Haptophytes	0.19 (0.16)	**0.14 (0.14)**	0.04 (0.05)	**0.06 (0.09)**	0.10 (0.11)
Cryptophytes	0.006 (0.006)	0.070 (0.088)	0.012 (0.026)	**0.002 (0.003)**	**0.039 (0.040)**
Silicoflagellates	0.15 (0.19)	0.25 (0.16)	0.25 (0.18)	0.06 (0.09)	0.18 (0.14)
C: Summer (weeks 23–35)	**2014 (a)**	**2015 (b)**	**2016 (c)**	**2017 (d)**	
Diatoms	0.23 (0.11)	0.20 (0.16)	0.13 (0.15)	0.16 (0.20)	
Prasinophytes	**0.17 (0.10)[d]**	**0.15 (0.10)[d]**	0.31 (0.19)	**0.38 (0.20)**	
Haptophytes	0.16 (0.11)	**0.22 (0.21)**	0.13 (0.13)	**0.09 (0.06)**	
Cryptophytes	0.07 (0.06)	0.15 (0.10)	0.10 (0.10)	0.09 (0.06)	
Silicoflagellates	0.32 (0.18)	0.25 (0.11)	0.27 (0.12)	0.19 (0.11)	
D: Autumn (weeks 36–48)	**2014 (a)**	**2015 (b)**	**2016 (c)**	**2017 (d)**	
Diatoms	0.35 (0.20)	**0.29 (0.20)[d]**	**0.34 (0.19)[d]**	**0.54 (0.14)**	
Prasinophytes	**0.11 (0.05)**	**0.17 (0.06)**	0.18 (0.08)	0.16 (0.04)	
Haptophytes	**0.28 (0.13)**	0.20 (0.07)	0.24 (0.15)	**0.13 (0.08)**	
Cryptophytes	0.07 (0.04)	0.10 (0.05)	0.06 (0.06)	0.10 (0.10)	
Silicoflagellates	**0.18 (0.12)[d]**	**0.22 (0.11)[d]**	0.18 (0.10)	**0.06 (0.07)**	

20–21), 2017 (weeks 13–22), and 2018 (weeks 11–15) (not shown). Surface ocean temperatures were variable during these episodes, and showed no uniform relationships with salinity. Week average salinity of 2014 was significantly higher compared to that of other years (Table 3). Seasonally averaged salinities showed no significant relationships with seasonally averaged ocean and air temperature. Air temperature showed no significant differences between grouped spring, summer, and winter weeks (Table 3). Springtime Chl *a* accumulation, expressed as the week number during which Chl *a* concentrations exceeded 0.1 and 1.0 mg m^{-3} showed maximal 8 weeks inter-annual variability (Table 4). Dynamics of springtime nutrient draw down showed maximal 2–3 weeks variability between observations of 2014, 2015, 2016, 2017, and 2018 (Table 4, Fig. 2). Seasonally grouped Chl *a* showed significant differences between years during winter (2014, 2016) and autumn (2015, 2016), but not during spring and summer (Table 3). Seasonally grouped phytoplankton taxonomic composition showed significant differences between years, but showed no correlations with ocean and air temperature, and salinity (Table 5). Turbidity showed pronounced variability in seasonal dynamics and magnitude (Supplement Table 2). High turbidity was observed during spring 2016 (week 22) and summer 2017 (week 28), whereas less pronounced seasonal dynamics were observed during 2014 and 2018.

Discussion

The time series of ocean physics, nutrients, and phytoplankton biomass and composition provided insight in the annual biogeochemical dynamics at the underwater observatory location on the southern shore of central Kongsfjorden. Phytoplankton dynamics at this site were ultimately driven by the seasonal cycle in solar elevation. Resulting changes in irradiance, air and ocean temperature, salinity, and density caused sharp seasonal contrasts in irradiance and nutrient availability. Furthermore, the long winter period of near darkness left a strong imprint on phytoplankton Chl *a* and composition, by decreasing the spring bloom inoculum, and increasing the relative abundance of diatoms, respectively. Early spring phytoplankton growth commenced during increasing ocean density and low air temperature, suggesting convective mixing at the start of the spring bloom, in agreement with maximal nutrient concentrations. The onset of surface stratification (on average week 15) amplified phytoplankton accumulation rates, nutrient draw down, and ocean surface heating. The initially weak springtime stratification was most strongly associated with seasonal warming of the water column. Spring bloom phenology was in accordance with that in the Fram Strait and the Atlantic sector of the Barents Sea, which show Chl *a* increases from wintertime lows during the first weeks of April (Stramska 2005; Oziel et al. 2017). Springtime stratification was further facilitated by atmospheric warming, thereby reducing the heat flux from the ocean. The Atlantic spring bloom conditions were modified by local freshwater discharge. The increasing ocean heat content intensified melt water discharge of sea ice and marine terminating glaciers, expanding a low salinity surface layer in the fjord in summer (weeks 23–35). From May onwards salinity and temperature driven stratification dominated at the underwater observatory, which reached maximal strength prior to the onset of the polar night (weeks 34–39). Summer stratification (estimated as the density difference relative to the maximal spring density prior to stratification during week 14) was on average sixfold stronger than during spring, restricting access to deep nutrients. This is in contrast to the weaker summertime stratification in the Fram Strait, and sea ice free parts of the Barents Sea, where wind mixing can periodically entrain nutrients in the surface ocean (Stramska 2005; Henley et al. 2020). As a consequence of the freshwater discharge, Kongsfjorden spring and summertime nutrient draw down patterns have a stronger resemblance to the sea ice covered northern Barents Sea shelf (Henley et al. 2020). Taxonomic composition differed markedly during spring and summer. Spring showed a strong contribution of diatoms (60%, relative to Chl *a*), which was roughly in agreement with early spring concentrations of silicic acid and nitrogen, based on which a 43% contribution of diatoms can be expected assuming drawdown of these nutrients in a 15–16 ratio, respectively (Brzezinski 1985). Increasing flagellated phytoplankton groups and the depletion of silicic acid and nitrate caused decreasing relative diatom abundance during spring. The cessation of the diatom bloom most likely provides early season carbon fluxes to benthic communities in Kongsfjorden, as opal is a main component in sediment trap studies in May (D' Angelo et al. 2018). Summertime nutrient limitation is suggested by changes in N : P ratios, as compared to winter and early spring. Nitrogen limitation was previously demonstrated for central Kongsfjorden during the early summer of 2015 (van de Poll et al. 2018, Kulk et al. 2019), in agreement with low N : P ratios (8.6) at that time. However, our time series also shows N : P ratios above the Redfield ratio, indicating periodic phosphorous limitation during summer as well. These elevated N : P ratios were driven by periodic high ammonium concentrations, suggesting that supply of regenerated nitrogen combined with strong microbial phosphate consumption also can cause phosphate limitation of phytoplankton. The flagellate dominated community, and peak bacteria and virus abundances suggest a high turnover of organic carbon and nutrient regeneration (Suttle 2007; Shelford and Suttle 2018). Flow cytometry showed high summertime abundances of small phytoplankton. Silicic acid increased after week 29, in concert with increased melt water discharge, which is a modest source of dissolved silicate but not nitrate (Meire et al. 2016; Halbach et al. 2019), coinciding with increased relative abundances of diatoms. Compared to the 10–20-fold spring time increase, summer Chl *a* dynamics were less pronounced. Chl *a* peaks (2–5 mg Chl *a* m^{-3}) were observed up to August (week 34), whereas autumn Chl

a concentration declined sharply, despite irradiance levels similar to those during the early stages of the spring bloom. Possibly, shortening day length caused declining growth rates, while loss factors such as grazing and viral lysis continued. With stratification still in place strong coupling between the grazer community and phytoplankton can be expected (Lindemann and John 2014). A similar coupling may occur with viruses, although they are also vulnerable to abiotic variables such as passive absorption to glacial sediment particles (Mojica and Brussaard 2014; Maat et al. 2019a, 2019b), which increase in load during summer due to glacial melt and river run-off (Pavlov et al. 2019). Indeed, summertime turbidity was on average twofold higher as compared to the first 8 weeks of the spring. This also coincided with higher nitrification (bacterial conversion of ammonium released by decomposing organic matter to nitrate and nitrite), a process that is known to be photosensitive (Guerrero and Jones 1996). Declining algal biomass was followed by a surface nitrification peak during the first five weeks of the polar night.

Declining air temperature during the autumn and winter increase the heat flux from the ocean to the atmosphere. Ocean cooling and reduced freshwater discharge increased surface density, consistent with an expanding mixed layer, thereby entraining higher nutrient concentrations in the surface ocean. This process terminated with the onset of stratification during the following spring. During early spring Chl *a*, and phytoplankton, bacterial and virus abundances reached a minimum. Bacteria and virus abundances were strongly associated with phytoplankton abundance and Chl *a*. Therefore, in contrast to summer, the low winter and early spring concentrations of phytoplankton and bacteria limit the effectiveness of heterotrophic and mixotrophic life styles during the polar night. Indeed, flagellated phytoplankton pigments declined during autumn and winter, causing a pronounced increase in diatom relative abundance. This suggests survival of diatoms during prolonged darkness, which is in agreement with dark survival experiments with diatoms and flagellates (Smayda and Mitchell-Innes 1974, van de van de Poll et al. 2019). Apart from reducing phytoplankton irradiance exposure, the expanding mixed layer can also entrain diatoms from deeper water layers and the ocean floor. Previously, regrowth of diatoms from sediment samples was demonstrated during the polar night (Hegseth et al. 2019). Dark survival allows diatoms to exploit early spring nutrient concentrations and irradiance, and may explain the fixed succession patterns of diatoms and flagellates at high latitude.

Inter-annual variability

During 2013–2018 inter-annual variability of ocean physics was considerable, but this could not be linked to variability in spring and summer nutrient concentrations, phytoplankton phenology, bloom magnitude (Chl *a*), and taxonomic composition. This suggests that changes in phytoplankton productivity and composition are not directly driven by these variables, but rather by seasonal changes in irradiance and solar heating/cooling of the water column, as supported by the correlations over the average annual cycle. Our observations do not support claims that warming of Kongsfjorden has changed taxonomic composition of phytoplankton blooms (apart from sea ice algae, which were not investigated). Inter-annual variability of ocean temperature (maximal 2.1°C) peaked during spring. We observed episodes of springtime Atlantic advection during all years except 2015. This suggests that advection of Atlantic water masses can be an inoculum of the spring bloom and can be a source of flagellated phytoplankton groups that show limited survival during prolonged darkness. Indeed, early spring phytoplankton composition of the WSC (Fram Straight) is a mixture of diatoms and *Phaeocystis pouchetii*, and other phytoplankton groups that are similar to our observations (Randelhoff et al. 2018). Identification of Atlantic advection beyond the spring bloom was not possible because surface salinity and temperature were strongly influenced by seasonal freshwater and heat fluxes. The additional lack of vertical and spatial resolution makes is difficult to resolve effects of Atlantic advection scenarios on springtime surface stratification and its effect on phytoplankton (Hegseth et al. 2019; Hop et al. 2019; Hop and Wiencke 2019). However, our data suggest that this may affect phenology but not taxonomic composition of the bloom. The glacial melt water cycle is predominantly driven by ocean heating and cooling, over 2013–2018 the annual fluctuation was 4.14°C for weekly averaged surface ocean temperature. Inter-annual differences during summer were maximally 1.7°C (between 2017 and 2018, the warmest and coldest summers in our time series). Calving of marine terminating glaciers has previously been correlated with ocean temperature (Luckman et al. 2015; Holmes et al. 2019). However, a direct link between inter-annual differences in summertime ocean temperature and salinity could not be established at the underwater observatory location, possibly, due to the variability in the depth of the freshwater layer (Divya David and Krishnan 2017) . Furthermore, the most pronounced freshwater outflow is confined to the northern shores, whereas internal fjord circulation influences the position of the monitoring location in the melt water gradient (Sundfjord et al. 2017). Our monitoring location is also close to the Bayelva river, and variability in its discharge is likely a function of air temperature, and therefore can also influence summertime salinity. The Bayelva plume is presumably also a source variability in turbidity observed at the underwater observatory site.

Kongsfjorden summer nutrient budgets are influenced by regeneration rates and by upwelled nutrients in close proximity of the glaciers (Lydersen et al. 2014, Halbach et al. 2019, Hopwood et al. 2020). Because summertime stratification is strong and presumably always constrains upward mixing of nutrients, inter-annual differences in summertime stratification may have limited consequences on nutrient availability. However, intensified glacial melting during warm years may

increase nutrient inventories during summer as compared to colder years by increased upwelling. Although nutrient upwelling of ammonium, nitrate, and phosphate have been observed near the glacier fronts in Kongsfjorden (van de Poll et al. 2018, Halbach et al. 2019), evidence for higher summer bloom magnitude as a result of increased temperature was not found. Downstream utilization of upwelled nutrients depends on irradiance conditions, and on wind or upwelling driven circulation patterns in the fjord (Sundfjord et al. 2017). These processes may underpin the patchiness of summer productivity and the Chl *a* peaks that were observed between weeks 30–35 (2014, 2015, 2016, and 2017). Remarkably, the late summer Chl *a* peaks were of equal magnitude as those observed during the spring–summer transition at the underwater observatory site.

Potential bias and limitations

The complexities of the Kongsfjorden system, and the relatively limited number of observed years constrained our ability to observe inter-annual variability of phytoplankton Chl *a*, composition, and their drivers. Furthermore, data density of the time series varied between variables, limiting our ability to detect inter-annual differences during the uncovered intervals. CHEMTAX taxonomic composition was calculated using groups that were previously observed in Kongsfjorden (van de Poll et al. 2016. van de Poll et al. 2018), and we found that this matched with microscopic observations of the 2014 and 2015 spring and summer blooms. Moreover, diatom relative abundance was in good agreement with independent observations of silicic acid concentrations. Previous research indicated that ratios of fucoxanthin and other marker pigments of diatoms and flagellates relative to Chl *a* were stable during 8 weeks of darkness (i.e., pigments declined equally, van de Poll et al. 2019). Pigments and CHEMTAX based phytoplankton composition provide coarse information, with no resolution beyond the taxonomic level. Furthermore, we cannot differentiate between cryptophyte pigments of flagellates and cryptophyte chloroplasts of the ciliate *Mesodinium rubrum*. Early spring stratification can be stronger in the glacier and sea ice influenced parts of the inner fjord as compared to central fjord, as was observed during the 2014 spring bloom (van de Poll et al. 2016). Since freshwater outflow predominantly follows the northern shore of Kongsfjorden, the observatory location may not capture the full extent of blooms initiated in the inner fjord. Low Chl *a* during the 2015 and 2018 spring bloom was not accompanied by a nutrient surplus, suggesting that these Chl *a* anomalies were not due to less productive blooms, but were caused by other factors. Although taxonomic composition of the underwater observatory samples matched that of samples of central Kongsfjorden (depth $\sim$ 300 m) of April–June 2014 and June 2015 (van de Poll et al. 2016, 2018), spring bloom peak Chl *a* concentrations were lower than those reported in deeper parts of central Kongsfjorden (Hegseth and Tverberg 2013; Poll et al. 2016). Possibly, peak concentrations were short lived and localized phenomena that were missed by our weekly sampling scheme. In addition to the above, variability of Chl *a* can reflect changes in cellular Chl *a* due to physiological adaptation (i.e., photoacclimation, nutrient limitation), and changes in cell size (Finkel 2001; van de Poll et al. 2005). The ratio of the most abundant photoprotective xanthophyll cycle pigments relative to Chl *a* (diadino and diatoxanthin) demonstrated differences in photoacclimation state during spring and summer (not shown). This is frequently observed in concert with reduced cellular Chl *a*, and changes in carbon: Chl *a* (Geider et al. 1997). Moreover, high abundance of small phytoplankton during summer can affect the carbon to Chl *a* ratio (Finkel 2001). Therefore, the strong seasonal oscillations in irradiance and nutrient conditions can be a source of variability in Chl *a* that do not reflect changes in carbon biomass.

Conclusion

Phytoplankton productivity in Kongsfjorden is driven by interactions between oceanic, atmospheric, and terrestrial processes, as indicated by strong correlations between biology and ocean physical and chemical properties over the average annual cycle. The observed years showed considerable variability of geochemical proxies and biology on inter-annual scale, but these could not be linked. We conclude that controls of phytoplankton growth (irradiance, nutrient concentrations, grazing, viral lysis) are strongly associated with the irradiance cycle and the presence of freshwater sources (glaciers, land fast ice, terrestrial run off). Therefore, the extreme seasonal changes in irradiance overwhelmingly dictate patterns of phytoplankton productivity and composition at this site, as compared to the inter-annual variability in ocean temperature and water mass composition in Kongsfjorden.

Links to data sets

Pigment data: https://doi.pangaea.de/10.1594/PANGAEA.878242 (under modification).

Observatory data: https://www.pangaea.de/?q=svalbard+underwater+observatory+fischer.

Meteorological data: https://doi.pangaea.de/10.1594/PANGAEA.914927.

References

Brussaard, C. P. D. 2004. Optimization of procedures for counting viruses by flow cytometry. Appl. Environ. Microbiol. **70**: 1506–1513. doi:10.1128/AEM.70.3.1506-1513.2004

Brzezinski, M. A. 1985. The Si:C:N ratio of marine diatoms: Interspecific variability and the effect of some environmental variables. J. Phycol. **21**: 347–357. doi:10.1111/j.0022-3646.1985.00347.x

Cottier, F., V. Tverberg, M. Inall, H. Svendsen, F. Nilsen, and C. Griffiths. 2005. Water mass modification in an Arctic

fjord through cross-shelf exchange: The seasonal hydrography of Kongsfjorden, Svalbard. J. Geophys. Res. **110**: (C12) doi:10.1029/2004jc002757

Divya David, T., and K. P. Krishnan. 2017. Recent variability in the Atlantic water intrusion and water masses in Kongsfjorden, an Arctic fjord. Polar Science **11**: 30–41. doi:10.1016/j.polar.2016.11.004

D'Angelo, A., F. Giglio, S. Miserocchi, A. Sanchez-Vidal, S. Aliani, T. Tesi, A. Viola, M. Mazzola, and L. Langone. 2018. Multi-year particle fluxes in Kongsfjorden, Svalbard. Biogeosciences **15**: 5343–5363. doi:10.5194/bg-15-5343-2018

Finkel, Z. V. 2001. Light absorption and size scaling of light limited metabolism in marine diatoms. Limnol. Oceanogr. **46**: 86–94. doi:10.4319/lo.2001.46.1.0086

Fischer, P., M. Schwanitz, R. Loth, U. Posner, M. Brand, and F. Schröder. 2016. First year of the new AWIPEV-COSYNA observatory in Kongsfjorden, Spitsbergen. Ocean Sci. Discuss. **52**: 1–34. doi:10.5194/os-2016-52

Fischer, P., and others. 2020. Operating cabled underwater observatories in rough shelf-sea environments: A technological challenge. Front. Mar. Sci. **7**: 13. doi:10.3389/fmars.2020.00551

Geider, R. J., H. L. Macintyre, and T. Kana. 1997. Dynamic model of phytoplankton growth and acclimation: Responses of the balanced growth rate and the chlorophyll a:carbon ratio to light, nutrient-limitation and temperature. Mar. Ecol. Prog. Ser. **148**: 187–200. doi:10.3354/meps148187

Grasshoff, K. 1983. Determination of nitrate, p. 143–150. *In* K. Grasshoff, M. Erhardt, and K. Kremeling [eds.], Methods of seawater analysis. Weinheim, Germany: Verlag Chemie.

Guerrero, M. A., and R. D. Jones. 1996. Photoinhibition of marine nitrifying bacteria. I. Wavelength-dependent response. Mar. Ecol. Prog. Ser. **141**: 183–192.

Guruvayoorappan, H., A. Miettinen, D. V. Divine, M. Moros, L. C. Orme, and R. Mohan. 2020. Ocean surface warming in Krossfjorden, Svalbard, during the last 60 years. Arktos **6**: 1–13. http://dx.doi.org/10.1007/s41063-019-00071-x

Halbach, L., M. Vihtakari, P. Duarte, A. Everett, M. A. Granskog, H. Hop, H. M. Kauko, S. Kristiansen, et al., 2019. Tidewater glaciers and bedrock characteristics control the phytoplankton growth environment in a fjord in the arctic. Frontiers in Mar. Sci. **6**: 1–18. doi:10.3389/fmars.2019.00254

Hegseth, E. N., and V. Tverberg. 2013. Effect of Atlantic water inflow on timing of the phytoplankton spring bloom in a high Arctic fjord (Kongsfjorden, Svalbard). J. Mar. Syst. **113–114**: 94–105. doi:10.1016/j.jmarsys.2013.01.003

Hegseth, E. N., P. Assmy, J. M. Wiktor, J. Wiktor Jr., S. Kristiansen, E. Leu, V. Tverberg, T. M. Gabrielsen, et al. 2019. Phytoplankton seasonal dynamics in Kongsfjorden, Svalbard and the adjacent shelf. *In* H. Hop and C. Wiencke [eds.], The ecosystem of Kongsfjorden, Svalbard. Advances in Polar Ecology, vol. 2. Springer. doi:10.1007/978-3-319-46425-1_5.

Helder, W., and R. T. P. De Vries 1979. An automatic phenol-hypochlorite method for the determination of ammonia in sea- and brackish waters. Neth. J. Sea Res. **13**: 154–160.

Henley, S. F., M. Porter, L. Hobbs, J. Braun, R. Guillaume-Castel, E. J. Venables, E. Dumont, and F. Cottier. 2020. Nitrate supply and uptake in the Atlantic Arctic Sea ice zone: Seasonal cycle, mechanisms and drivers. Phil. Trans. R. Soc. **378**: 1–21. doi:10.1098/rsta.2019.0361.

Higgins, H. W., S. W. Wright, and L. Schlüter. 2011. Quantitative interpretation of chemotaxonomic pigment data, p. 257–313. *In* S. Roy, C. A. Llewellyn, E. S. Egeland, and G. Johnsen [eds.], Phytoplankton Pigments: Characterization, Chemotaxonomy and Applications in Oceanography. UK: Cambridge University Press. doi:10.1017/CBO9780511732263.010

Holmes, F. A., N. Kirchner, J. Kuttenkeuler, J. Krützfeldt, and R. Noormets. 2019. Relating ocean temperatures to frontal ablation rates at Svalbard tidewater glaciers: Insights from glacier proximal datasets. Sci. Rep. **9**: 9442. doi:10.1038/s41598-019-45077-3

Hop, H., and C. Wiencke. 2019. The ecosystem of Kongsfjorden, Svalbard. *In* H. Hop and C. Wiencke [eds.], Advances in polar ecology, vol. 2. Springer. doi:10.1007/978-3-319-46425-1_1

Hop, H., F. Cottier, and J. Berge. 2019. Autonomous marine observatories in Kongsfjorden, Svalbard. *In* H. Hop and C. Wiencke [eds.], The ecosystem of Kongsfjorden, Svalbard, Advances in polar ecology, vol. 2. Springer. doi:10.1007/978-3-319-46425-1_13

Hopwood, M. J., D. Carroll, T. Dunse, A. Hodson, J. M. Holding, J. L. Iriarte, S. Ribeiro, E. Achterberg, and others. 2020. How does glacier discharge affect marine biogeochemistry and primary production in the Arctic? Cryosphere **14**: 1347–1383. doi:10.5194/tc-14-1347-2020

Kortsch, S., R. Primicerio, F. Beuchel, P. E. Renaud, J. Rodrigues, O. J. Lønne, and B. Gulliksen. 2012. Climate-driven regime shifts in Arctic marine benthos. Proc. Natl. Acad. Sci. U. S. A. **109**: 14052–14057. doi:10.1073/pnas.1207509109

Kulk, G., W. H. van de Poll, and A. G. J. Buma. 2019. Photophysiology of nitrate limited phytoplankton communities in Kongsfjorden, Spitsbergen. Limnol. Oceanogr. **63**: 2606–2617. doi:10.1002/lno.10963

Lindemann, C., and M. A. S. John. 2014. A seasonal diary of phytoplankton in the North Atlantic. Front. Mar. Sci. **1**: 37. doi:10.3389/fmars.2014.00037

Luckman, A., D. I. Benn, F. Cottier, S. Bevan, F. Nilsen, and M. Inall. 2015. Calving rates at tidewater glaciers vary strongly with ocean temperature. Nat. Commun. **6**: 8566. doi:10.1038/ncomms9566

Lydersen, C., P. Assmy, S. Falk-Petersen, J. Kohler, K. M. Kovacs, M. Reigstad, H. Steen, S. H. Hallvard, and others. 2014. The importance of tidewater glaciers for marine mammals and seabirds in Svalbard, Norway. J. Mar. Sys. **129**: 452–471. doi:10.1016/j.jmarsys.2013.09.006

Maat, D. S., R. J. W. Visser, C. P. D. Brussaard. 2019*a*. Virus removal by glacier-derived suspended fine sediment in the Arctic. J. Exp. Mar. Biol. Ecol., **521**. doi:10.1016/j.jembe.2019.151227, 151227

Maat, D. S., M. A. Prins, and C. P. D. Brussaard. 2019*b*. Sediments from Arctic tide-water glaciers remove coastal marine viruses and delay host infection. Viruses **11**: 123. doi:10.3390/v11020123

Mackey, M. D., H. W. Higgins, D. J. Mackey, and S. W. Wright. 1996. CHEMTAX – A program for estimating class abundances from chemical markers: Application to HPLC measurements of phytoplankton. Mar. Ecol. Prog. Ser. **144**: 265–283. doi:10.3354/meps144265

Marie, D., F. Partensky, D. Vaulot, and C. P. D. Brussaard. 2001, 2001. Enumeration of phytoplankton, bacteria, and viruses in marine samples, p. 11.11.1–11.11.15. *In* Current protocols in cytometry, v. **10**. NJ, USA: John Wiley & Sons. doi:10.1002/0471142956.cy1111s10

Maturilli, M., I. Hanssen-Bauer, R. Neuber, M. Rex, and K. Edvardsen. 2019. The atmosphere above Ny-Ålesund: Climate and global warming, ozone and surface UV radiation. *In* H. Hop and C. Wiencke [eds.], The ecosystem of Kongsfjorden, Svalbard. Advances in polar ecology, vol. 2. Springer. doi:10.1007/978-3-319-46425-1_2

Meire, L., and others. 2016. High export of dissolved silica from the Greenland ice sheet. Geophys. Res. Lett. **43**: 9173–9182. doi:10.1002/2016GL070191

Mojica, K. D., and C. P. D. Brussaard. 2014. Factors affecting virus dynamics and microbial host–virus interactions in marine environments. FEMS Microbiol. Ecol. **89**: 495–515. doi:10.1111/1574-6941.12343

Murphy, J., and J. P. Riley. 1962. A modified single solution method for the determination of phosphate in natural waters. Anal. Chim. Acta **27**: 31–36. doi:10.1016/S0003-2670(00)88444-5

Oziel, L., G. Neukermans, M. Ardyna, C. Lancelot, J.-L. Tison, P. Wassmann, J. Sirven, D. Ruiz-Pino, and J.-C. Gascard. 2017. Role for Atlantic inflows and sea ice loss on shifting phytoplankton blooms in the Barents Sea. JGR Oceans **122**: 5121–5139. doi:10.1002/2016JC012582

Pavlov, A. K., E. Leu, D. Hanelt, I. Bartsch, U. Karsten, S. R. Hudson, J. C. Gallet, F. Cottier, J. and others. 2019. The underwater light climate in Kongsfjorden and its ecological implications. In: Hop, H., Wiencke, C. (eds) The ecosystem of Kongsfjorden, Svalbard. Advances in polar ecology, vol. 2. Springer., doi:10.1007/978-3-319-46425-1_6

Pavlova, O., S. Gerland, and H. Hop. 2019. Changes in sea-ice extent and thickness in Kongsfjorden, Svalbard (2003–2016). *In* H. Hop and C. Wiencke [eds.], The ecosystem of Kongsfjorden, Svalbard. Advances in polar ecology, vol. 2. Springer. doi:10.1007/978-3-319-46425-1_4

Piquet, A. M. T., W. H. van de Poll, R. J. W. Visser, C. Wiencke, H. Bolhuis, and A. G. J. Buma. 2014. Springtime phytoplankton dynamics in the Arctic Krossfjorden and Kongsfjorden (Spitsbergen) as a function of glacier proximity. Biogeosciences **11**: 2263–2279. doi:10.5194/bg-11-2263-2014

van de Poll, W. H., D. S. Maat, P. Fischer, P. D. Rozema, O. B. Daly, S. Koppelle, R. J. W. Visser, and A. G. J. Buma. 2016. Atlantic advection driven changes in glacial meltwater: Effects on phytoplankton chlorophyll a and taxonomic composition in Kongsfjorden, Spitsbergen. Front. Mar. Sci. **3**: 1–11. doi:10.3389/fmars

van de Poll, W. H., G. Kulk, P. D. Rozema, C. P. D. Brussaard, R. J. W. Visser, and A. G. J. Buma. 2018. Contrasting glacial meltwater effects on post-bloom phytoplankton on temporal and spatial scales in Kongsfjorden, Spitsbergen. Elementa **6**: 1–13. doi:10.1525/elementa.307

van de Poll, W. H., E. Abdullah, R. J. W. Visser, P. Fischer, and A. G. J. Buma. 2019. Taxon-specific dark survival of diatoms and flagellates affects Arctic phytoplankton composition during the polar night and early spring. Limnol. Oceanogr. **65**: 903–914. doi:10.1002/lno.11355

Randelhoff, A., M. Reigstad, M. Chierici, A. Sundfjord, V. Ivanov, M. Cape, M. Vernet, J.-É. Tremblay, et al. 2018. Seasonality of the physical and biogeochemical hydrography in the inflow to the Arctic Ocean through Fram Strait. Front. Mar. Sci. **29**: 1–16. doi:10.3389/fmars.2018.00224

Shelford, E. J., and C. A. Suttle. 2018. Virus-mediated transfer of nitrogen from heterotrophic bacteria to phytoplankton. Biogeosciences **15**: 809–819. doi:10.5194/bg-15-809-2018

Smayda, T. J., and B. Mitchell-Innes. 1974. Dark survival of autotrophic, planktonic marine diatoms. Mar. Biol. **25**: 195–202. doi:10.1007/BF00394965

Soltwedel, T., E. Bauerfeind, M. Bergmann, A. Bracher, N. Budaev, K. Busch, A. Cherkashev, K. Fahl, and others. 2016. Natural variability or anthropogenically-induced variation? Insights from 15 years of multidisciplinary observations at the arctic marine LTER site HAUSGARTEN. Ecol. Indicat. **65**: 89–102. doi:10.1016/j.ecolind.2015.10.001

Stramska, M. 2005. Interannual variability of seasonal phytoplankton blooms in the north polar Atlantic in response to atmospheric forcing. J. Geophys. Res. **110**: C05016. doi:10.1029/2004JC002457

Sundby, T. S., K. F. Drinkwater, and O. S. Kjesbu. 2016. North Atlantic spring-bloom system-where the changing climate meets the winter dark. Front. Mar. Sci. **3**: 1–12. doi:10.3389/fmars.2016.00028

Sundfjord, A., J. Albretsen, Y. Kasajima, R. Skogseth, J. Kohler, C. Nuth, J. Skarðhamar, F. Cottier, and others. 2017. Effects of glacier runoff and wind on surface layer dynamics and Atlantic Water exchange in Kongsfjorden, Svalbard; a

model study. Estuar. Coast. Shelf Sci. **187**: 260–272. doi:10.1016/j.ecss.2017.01.015

Suttle, C. A. 2007. Marine viruses—Major players in the global ecosystem. Nat. Rev. Microbiol. **5**: 801–812.

Tverberg, V., R. Skogseth, F. Cottier, A. Sundfjord, W. Walczowski, M. E. Inall, E. Falck, O. Pavlova, and F. Nilsen. 2019. The Kongsfjorden transect: Seasonal and inter-annual variability in hydrography. *In* H. Hop and C. Wiencke [eds.], The ecosystem of Kongsfjorden, Svalbard. Advances in polar ecology, vol. 2, Springer. doi:10.1007/978-3-319-46425-1_3

van de Poll, W. H., M. A. van Leeuwe, J. Roggeveld, and A. G. J. Buma. 2005. Nutrient limitation and high irradiance reduce PAR and UV-induced viability loss in the Antarctic diatom *Chaetoceros brevis*. J. Phycol. **41**: 840–850. doi:10.1111/j.1529-8817.2005.00105.x

Van Heukelem, L., and C. S. Thomas. 2001. Computer-assisted high-performance liquid chromatography method development with applications to the isolation and analysis of phytoplankton pigments. J. Chromatogr. A **910**: 31–49. doi:10.1016/S0378-4347(00)00603-4

van Leeuwe, M. A., L. A. Villerius, J. Roggeveld, R. J. W. Visser, and J. Stefels. 2006. An optimized method for automated analysis of algal pigments by HPLC. Mar. Chem. **102**: 267–275. doi:10.1016/j.marchem.2006.05.003

Acknowledgments

We thank the AWIPEV technicians and station leader for sample collection at the underwater observatory, without their dedicated sampling this project would not be possible. We thank Marion Maturilli for sharing AWIPEV irradiance and air temperature measurements. This is a contribution to NWO project 866.12.408 (Buma) and project number 866.12.404 (Brussaard).

Conflict of interest

None declared.

Submitted 05 June 2020
Revised 25 September 2020
Accepted 03 December 2020

Associate editor: Heidi Sosik